Geoderma 427 (2022) 116126

Contents lists available at ScienceDirect

Geoderma

journal homepage: www.elsevier.com/locate/geoderma

Capturing water repellency cessation time by means of characteristic time method

Nasrollah Sepehrnia *, Jörg Bachmann

Institute of Soil Science, Leibniz Universität Hannover, Herrenhäuser Str. 2, D-30419 Hannover, Germany

ARTICLE INFO

Handling Editor: Haly Neely

Keywords:
Water repellency breakdown
Characteristic time method
Capillary infiltration dynamics
Contact angle
Persistence
Molecular interfacial properties

ABSTRACT

Persistence of water repellency is a significant physical key factor that governs water infiltration into unsaturated soil. We investigated water and ethanol infiltration using the characteristic time method (CTM), repellency index (*RI*), and the contact angle (CA) behavior for a comprehensive assessment on soil water repellency (SWR). We analyzed the impact of soil structure and thermal and wetting–drying treatments on water and ethanol infiltration. The first objective was to evaluate the CTM for water-repellent soils by partitioning characteristic and gravity infiltration behavior (I_{char} and I_{grav}) and to evaluate parameters like infiltration beginning (t_b) and gravity times (t_{char} and t_{grav}). The second objective was to characterize the CTM estimated water sorptivity (S_w), either as the S_{ww} (the hydrophilic state water sorptivity) or the S_{wh} (the hydrophobic state water sorptivity) to improve the calculation of water repellency cessation time (WRCT). Three soils with initial contact angles (CA_i) of 18°, 60°, and 90° (20 °C ± 3 °C) were additionally heated to temperatures of 40 °C and 60 °C resulting in CA_{T40}: of 23.6°, 56.4°, and 97.3° and CA_{T60} of 18.5°, 88.0°, and 126.6°. The wetted state CA was determined for a wetting- and a rewetting-infiltration cycle (CA_{we} and CA_{rewe}) under –2 cm tension, followed by air-drying and further CA measurements ($CA_{air\text{-}dried}$). There was significant agreement ($R^2 > 0.95$) between the S_w evaluated by CTM and the S_{wh}, and excellent correspondence between t_{char} and the t_b. The relations between S_e, *RI*, CA_{we}, CA_{rewe}, $CA_{air\text{-}dried}$, and WRCT clearly showed dynamics and reversibility of SWR and also its dependence on persistence, even for the air-dried 20 °C soil with small CA_i. Persistence of SWR as characterized by the time components resulted in a long flow transition state (*i.e.,* time development and respective changing relevance of capillary and gravity forces). Hence, missing experimental data has to be considered as the main barrier for modeling approaches. Further research is necessary to improve flexibility of the CTM code to reliably estimate S_w and S_{wh} with respect to persistence of SWR.

1. Introduction

Extreme climatic processes, such as long-term drought, extreme precipitation, and frequent wet-dry cycles can be enhanced by climate change effects (Arye et al., 2007; Goebel et al., 2011; Lesk et al., 2016). In this context, water repellency strongly influences soil properties of some soils from micro- to macro-scales (Daniel et al., 2019; Mao et al., 2019). The SWR phenomenon, which is moisture-dependent, can affect many of soil physical and hydrophysical properties (Bachmann et al., 2007, 2016; de Jonge et al., 2007). Therefore, it is useful to define adequate experimental tools that can explicitly and insightfully evaluate SWR dynamics.

The methods to assess SWR are usually based on soil hydraulic behavior and are related to the concepts of extent/intensity and its time behavior, which is defined as persistence of water repellency (Daniel et al., 2019; Hermansen et al., 2019; Iovino et al., 2018). Both soil properties can be determined by the wetting process immediately after water meets soil particles. The persistence of SWR is commonly derived only for hydrophobic soils (*i.e.,* contact angle > 90°) and is defined as the stability of the respective water repellency with time after contact with water. Previously, it was mainly assessed by the empirical water drop penetration time (WDPT) test, (Dekker and Ritsema, 1994; Ritsema et al., 1998), indicating persistency for hydrophobic soil in contact with water under high (positive) pressure conditions of the droplet-soil interface related to atmospheric pressure. Hence, this test determines only how long strong water repellency persists in the contact area of a water droplet (Dekker et al., 2009).

The WDPT method is proposed to simultaneously measure initial strong water repellency and persistence (Doerr, 1998; Doerr and

* Corresponding author.
E-mail address: sepehrnia@ifbk.uni-hannover.de (N. Sepehrnia).

https://doi.org/10.1016/j.geoderma.2022.116126
Received 27 August 2021; Received in revised form 19 July 2022; Accepted 18 August 2022
Available online 6 September 2022
0016-7061/© 2022 Elsevier B.V. This is an open access article under the CC BY-NC-ND license (http://creativecommons.org/licenses/by-nc-nd/4.0/).

Nomenclature

List of symbols, acronyms and units

Parameter	Definition unit
SWR	Soil water repellency –
WS	Wettable soil –
SRS	Subcritically water-repellent soil–
WRS	Water-repellent soil –
CTM	Characterized time method –
CA	Contact angle °
CA_i	Initial contact angle °
CA_{we}	Contact angle for the wetting process °
CA_{rewe}	Contact angle for the rewetting process °
CA_{infil}	Contact angles of the wetting and rewetting process °
CA_{T40}	Contact angle after thermal treatment at 40 °C °
CA_{T60}	Contact angle after thermal treatment at 60 °C °
$CA_{air\text{-}dried}$	Contact angle after air drying samples °
WRCT	Water repellency cessation time h
S_w	Soil water sorptivity cm $h^{-0.5}$
S_{wCTM}	Water sorptivity estimated from CTM cm $h^{-0.5}$
S_{ww}	Soil water sorptivity at hydrophilic state cm $h^{-0.5}$
S_{wh}	Soil water sorptivity at hydrophobic state cm $h^{-0.5}$
S_e	Soil ethanol sorptivity cm $h^{-0.5}$
S_{eCTMs}	Ethanol sorptivity estimated from CTM cm $h^{-0.5}$
RI	Repellency index –
RI_m	Modified repellency index –
t_b	Infiltration beginning time h
t_{char}	A given characteristic time which falls between zero and t_{grav} h
t_{grav}	The time when gravity and capillarity forces have exactly the same impact on infiltration h
I_{char}	The cumulative infiltration at time equal to t_{char} cm
I_{grav}	The cumulative infiltration at time equal to t_{grav} cm
α	A soil-dependent shape factor being negative for the sorptivity component and positive for the gravity component h^{-1}
ω	Contribution of the gravity component to the infiltration process –

Thomas, 2000; Flores-Mangual et al., 2011; Hardie et al., 2012); it assumes that the greater the water drop penetration time, the greater the soil hydrophobicity (Doerr, 1998; Flores-Mangual et al., 2011). This test does not distinguish between persistence and degree of water repellency because it only considers hydrophobic soil conditions above or close to contact angles of 90° and does not consider the wide range of subcritical repellency for CA smaller than 90°. The advantage of the WDPT test is that it is a simple and inexpensive method that can be directly related to water infiltration and it could be used in the field for ambient soil water content and in the laboratory under well controlled conditions.

The WDPT test is sensitive for strong water repellent soils but insensitive for so-called subcritical water-repellency levels which are, as recent research shows, a common feature of many soils and not very well investigated regarding their impact on soil processes (Bachmann et al., 2007). Therefore, the WDPT is only able to detect persistence of hydrophobic soils and/or the transition of hydrophobic state to subcritical repellency, which is only a small window of possible soil wetting states (Bachmann et al., 2007). Additional drawbacks are that it could be time consuming - up to hours for some soils (Flores-Mangual et al., 2011).

The WDPT also tests the persistence under hydraulic pressure conditions that are unusual in soil for most wetting and redistribution processes. The hydraulic pressure and the vapor pressure underneath the positively curved droplet is, according to Kelvińs equation, significantly higher compared to the capillary pressure situation in unsaturated soil, which also refers to the lower water vapor pressure in equilibrium with the negatively curved water menisci. Drop forming positive pressure conditions (higher pressure related to atmosphere) seldom occur in soils (mostly at the wetting front of liquid fingers) due to instabilities of wetting fronts (saturation overshoot situations) at the soil surface under ponding conditions or at deeper located impermeable soil layers. The persistence estimated by WDPT doesn't represent the real persistence conditions in the entire soil matrix in general.

Another widespread method is the sessile drop method, which rates persistence in terms of sessile drop contact angles in the range between 0° and 180°, hence characterizing the entire spectrum from completely wettable soils to extreme hydrophobic soils. The state of soil wettability based on contact angle (CA) is categorized in three groups; hydrophobic (strong water-repellency, CA > 90°), subcritical or moderate water repellency (CA < 90°, > 0°), and perfect wettability (CA = 0°) (Bachmann et al., 2000).

Attempts have recently been made to assess the persistence of SWR utilizing the concept of water repellency cessation time (WRCT) by a single water infiltration test under negative capillary pressure conditions (the Hockey-stick method) (Lichner et al., 2013; Sepehrnia et al., 2016, 2017). The WRCT is the time span in which soil, in contact with water, shows water repellency before disappearance, *i.e.,* due to low persistence or increasing water content (Lichner et al., 2013; Sepehrnia et al., 2016, 2017). The WRCT is estimated from the "Hockey-stick-like" relationship in the cumulative water infiltration test by fitting Philip's (1957) model equation (*i.e.,* Sharma et al.,1980) as shown by Lichner et al. (2013). As proposed by Lichner et al. (2013), the cumulative water infiltration '*I*' versus square root of time '*t*' is separated into two stages starting from the water sorptivity for the hydrophobic state (S_{wh}) followed by the water sorptivity for the wettable status (S_{ww}). Based on this, Sepehrnia et al.(2016) proposed a modified repellency index RI_m (S_{ww}/S_{wh}) to capture the extent and persistence information simultaneously.

The extent of SWR is traditionally determined by the conventional repellency index, RI (S_e/S_w), defined as 1.95 times the ratio of ethanol (S_e) and water (S_w) sorptivity (Hallett and Young, 1999). Soil sorptivity (S) is estimated by plotting cumulative infiltration I versus square root of time t similar to Philip's equation (1957), *i.e.,* Sharma et al., (1980). The RI measures how strong capillarity forces of a water repellent porous medium are reduced with time compared to wettable counterpart (Alagna et al., 2019).

Overall, two questions are still pending about the procedures to evaluate RI_m and RI:

First, for RI_m different situations have to be distinguish: if water repellency is absent, the values for S_{ww} indicate the behaviour of a completely wetting liquid (CA = 0) in extreme cases. In all other cases, the RI_m indicates the transition from hydrophobic to water repellent, but the latter does not necessarily include complete wetting conditions (i.e., maximum S_{ww}, or a contact angle CA = 0). It would be helpful to test the capability of this method regarding whether it is possible to differentiate between hydrophobicity and water repellency and also between water repellency and complete wettability. For instance, Alagna et al. (2019) and Sepehrnia et al. (2016, 2017) found that the WRCT was correlated to WDPT and concluded that WRCT is essentially a measure of the persistence of SWR, but with a better resolution in the subcritical wetting states, indicating that complete wetting conditions may not be observed for extreme water repellent soils after wetting.

Second the question is pending if estimations of the extent of SWR by the usual early-time infiltration equation may overestimate SWR with regard to neglected soil-specific effects of the relation between gravity driven versus lateral capillary fluxes (Alagna et al., 2019). It is evident from the underlying principles of the WDPT test that only a part of the

transition process from restricted wettability and its conversion to better wettable stages can be detected by WDPT. When infiltration-based methods are considered there is still substantial arbitrariness in deciding if a plausibly linear relationship for S exists that leads to uncertainty effects for the estimated values depending on the choice of methods (Rahmati et al., 2020).

Rahmati et al. (2020) proposed the characterized time method (CTM) to quantify S and K_s (saturated hydraulic conductivity) values based on data from 1D-infiltration experiments (Rahmati et al., 2020) to circumvent arbitrariness in deciding if a plausible linear relationship for S exist. However, it was not defined if the CTM estimated S is either S_{ww} (hydrophilic state water sorptivity) or S_{wh} (hydrophobic state water sorptivity). Considering that real micro-hydraulic situations in soil may be influenced by the extent of water repellency and by their specific time-depending transition stages for persistence, it is evident that processes like infiltration behavior including the effect of capillary driven versus gravity driven water flow are also directly affected. Overall, this raises the question how, during infiltration, (especially under capillary pressure conditions) wettability transition processes affect the observed hydraulic situation in soils. Regarding cumulative infiltration curves, Sepehrnia et al. (2020) characterized a three-phase infiltration rate trend versus time in all experiments indicating a general trend (Fig. 1a). This trend is also obvious in the previous studies in which SWR and water infiltration were addressed (Lichner et al., 2013; Beatty and Smith, 2013, 2014; Alagna et al., 2019).

We thus hypothesized that the relevant components of water repellency cessation time (WRCT), S_{wh}, and S_{ww}, may be better characterized with the following objectives; (i) model water and ethanol infiltration using the CTM theory to evaluate suitability and flexibility of the proposed method for different soils with various levels of extent and persistence of water repellency; (ii) characterize the CTM estimated S_w in term of S_{ww} or the S_{wh} to improve WRCT estimation. For these, we investigated SWR changes of soils in terms of *RI* and CA as influenced by soil structure, and thermal and wetting–drying treatments followed by analyzing the data using the CTM code.

2. Theory

For an infiltration test, the gravity time, t_{grav}, needed to predict S and K_s, is defined as the time when gravity and capillarity forces have exactly the same effect on infiltration (Fig. 1b). In this procedure, t_{grav} is also used to give an idea about the transition time span that separates the

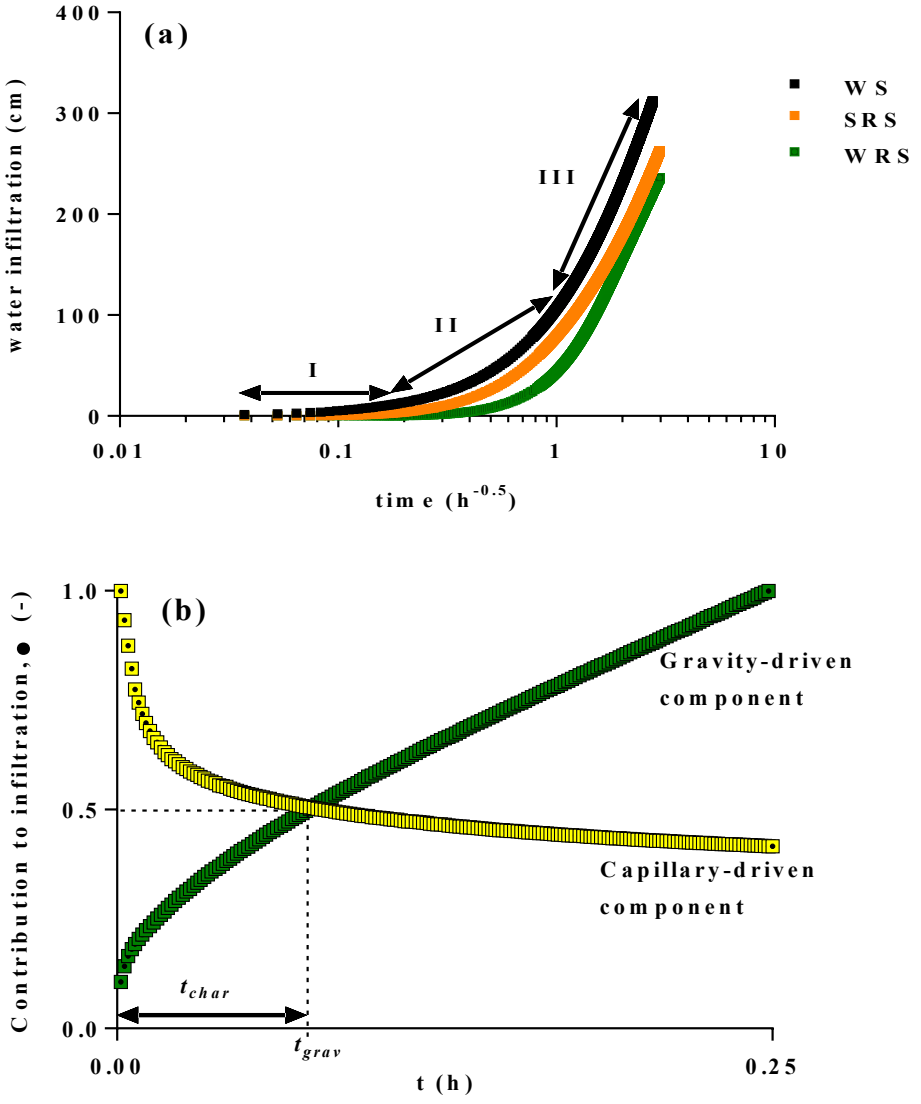

Fig. 1. (a) Examples of water infiltration into the studied soils (WS: wettable soil, SRS: subcritically water-repellent soil, and WRS: water-repellent soil), (b) time-development of capillary- and gravity-driven components to cumulative infiltration. For $\omega = 0.5$, steady state water flow is established and the time components of CTM modeling (*i.e.*, t_{char} and t_{grav}) are obtained.

steady-state of water infiltration from the transient regime (Philip, 1969; Lassabatère et al., 2006). The CTM takes the Philip's (1957) fifth-term equation (Eq. (1)) to remedy the time validity problem of the first- and two-terms equations which are widely applied for short time experiments (*e.g.,* Sharma et al., 1980), and considers Haverkamp et al.'s (1994) model to depict the individual contribution (W) of each term to the infiltration process:

$$I(t) = c(1)t^{1/2} + c(2)t + c(3)t^{3/2} + c(4)t^{2} + c(5)t^{5/2} \quad (1)$$

where $c(1) = S$, $c(2) = \frac{2-\beta}{3}K_s$, $c(3) = \frac{1}{9}(\beta^2 - \beta + 1)\frac{K_s^2}{S}$,

$$c(4) = \frac{2}{135}(\beta - 2)(\beta + 1)(1 - 2\beta)\frac{K_s^3}{S^2}, c(5) = \frac{1}{270}(\beta^2 - \beta + 1)^2\frac{K_s^4}{S^3}$$

In Eq. (1) t is time, and β (dimensionless) an integral infiltration constant that is either fixed at 0.6 (Rahmati et al., 2020) or that can be adjusted soil specifically (see Haverkamp et al., 1994). Rahmati et al. (2020) considered β fixed at 0.6. If both the right and left sides of Eq.1 are divided by $I(t)$, the following equation illustrates the iterative and normalized contribution of each term (W_i) to the infiltration process:

$$W_i = \frac{c(i)t^{i/2}}{I(t)}, \quad i = 1, 2, ..., 5 \quad (2)$$

where $W_1 + W_2 + W_3 + W_4 + W_5 = 1$.

In Eq. (2), it is assumed that the contribution of the higher order terms (orders > 5) are negligible, thus within the validation time interval the approximation is related to the first five-terms of the expansion. Rahmati et al. (2020) proved that by advancing in time, any decrease in the contribution of sorptivity component results in a corresponding increase in the contributions of the gravity components (Fig. 1b). They plotted the contributions of different components (W1 to W5) to a simulated infiltration curve for known values of S and K_s and obtained an exponential form for the contribution of the sorptivity (or gravity) component vs time (Eq. 3).

$$W = e\alpha^{t} \quad (3)$$

where α (h^{-1}) is a soil-dependent shape factor being negative for the sorptivity component and positive for the gravity component. As a consequence, once t_{grav} has been identified, the S and K_s can be estimated from cumulative infiltration data using the iterative procedures called CTM-I and CTM-K_s, respectively. We address the CTM-I functionality mechanism below and refer readers to Rahmati et al. (2020) to find the two approaches and the advantages in detail. In short, the CTM-I considers a given characteristic time (t_{char}) that falls between zero and t_{grav} with regard to its related weight, ω (Eq. 4):

$$\text{at } 0 < t_{char} \le t_{grav} \Rightarrow W_1 = 1 - \omega \Rightarrow \frac{S\sqrt{t_{char}}}{I_{char}} = 1 - \omega \quad (4)$$

where ω is the contribution of the gravity component to the infiltration process, so 1 − ω is the contribution of the first component to the infiltration process, and I_{char} is the cumulative infiltration at time equal to t_{char}. In Eq. 4, if t_{char} is equal to t_{grav} ($t_{char} = t_{grav}$), ω will be equal to 0.5. For $t_{char} < t_{grav}$, smaller values of ω will be applied, whereas for $t_{char} \approx 0$, ω = 0 will be applied. The t_{char} can be related to t_{grav} given in Eq. 5:

$$t_{char} = \kappa t_{grav}, \text{ where } 0 < \kappa \leqslant 1 \quad (5)$$

Rearranging Eq. 4 produces the final solution for S which provides prediction of S based t_{char} (Eq. (6)):

$$S = (1 - \omega)\frac{I_{char}}{\sqrt{t_{char}}} \quad (6)$$

Therefore, the CTM-I procedure determines the $t_{char} - I_{char}$ set and ω from field- or laboratory measured 1D infiltration data to compute S and K_s. For the latter, as mentioned earlier, the CTM-K_s should be applied (Rahmati et al., 2020). The original CTM code written in Python 3 (Van Rossum and Drake, 2009) is available in Rahmati et al. (2020). A flowchart illustrating the characteristic time method coupled with the iterative procedure (CTM-I) is presented in supplementary data.

3. Materials and methods

3.1. Soil sample preparation and studied area

The sampling site was Grinderwald beech forest (*Fagus sylvatica L.*) (52°49.834′N 10°18.967′E), in Lower Saxony, Northern Germany. The site was established in 1916 and replaced a former pine forest (Liebmann et al., 2022). Mean annual temperature and precipitation are 9.7 °C and 762 mm, respectively (Liebmann et al., 2022). Undisturbed and disturbed samples were taken from three soil pits, hereafter called water-repellent (0–5 ± 2 cm), subcritically water-repellent (10–20 cm), and wettable (20–40 cm) soil, differentiated and classified according to our previous studies (*e.g.,* Sepehrnia et al., 2020). The depths are the average of the layers in the site. We tried to minimize the heterogeneities of sampling location and have unique samples particularly for the surface layer with regard to plant debris and litter. The undisturbed soils were thus sampled using metal cores (6 × 8.5 cm, 340 cm^3). The disturbed samples were gently passed through a 2-mm sieve at field water content and filled into the given cores after air drying at room temperature (20 °C ± 3 °C). Bulk densities were adjusted to corresponding undisturbed samples (Sepehrnia et al., 2020). The air-dried cores including disturbed and undisturbed samples were separately exposed to thermal treatments at 40 °C and 60 °C in a drying oven until reaching constant weight followed by a further 24 h of drying. The sample weights after 24 h were considered the reference for each of the thermal treatments. Other chemical and physical properties of the studied soils are presented in Sepehrnia et al. (2020).

3.2. Infiltration; wetting and rewetting

Water and ethanol infiltration experiments were carried out under –2 cm tension using a microinfiltrometer (with a 3-mm inner diameter) modified by Sepehrnia et al. (2020). This near zero tension was selected because of: i) the strong positive correlation between sorptivity and surface elemental composition (i.e., oxygen-to-carbon ratio) (Sepehrnia et al., 2020); ii) reduced macropore flow (Hallett et al., 2001; Beatty and Smith, 2013, 2014; Lichner et al., 2013); iii) making water infiltration for severe water repellent conditions possible due to a pressure close to atmospheric pressure (Sepehrnia et al., 2020).

The volumes of infiltrated liquids were automatically recorded at 5 s intervals using a four-digit balance (Kern, Germany) for the entire experiment time until 22 and 17 mL of water and ethanol, respectively were infiltrated (*i.e.,* so called first wetting cycle), The wet samples were immediately weighted and again air-dried (20 °C room temperature) until reaching the original weight. The latter process was prolonged with regard to the water repellency of the samples. The second run of infiltration tests (*i.e.,* so called rewetting) was performed similar to the wetting process until the same volume of the liquids penetrated into the soils. Triplicate measurements were performed for all experiments.

3.3. Water repellency index (RI) and cessation time (WRCT)

The samples were examined to estimate WRCT from the first-term Philip's infiltration equation (Philip, 1957) (Eq. (7)), so that the point of intersection of two straight lines for the cumulative infiltration, representing the $I = t^{1/2}$ relationships for hydrophobic state changing to a state of hydrophilic was considered the WRCT (Lichner et al., 2013; Sepehrnia et al. 2016).

$$I(t) = St^{1/2} \quad (7)$$

where I, S (i.e., $c(1)$ in Eq. (2)), and t are cumulative infiltration,

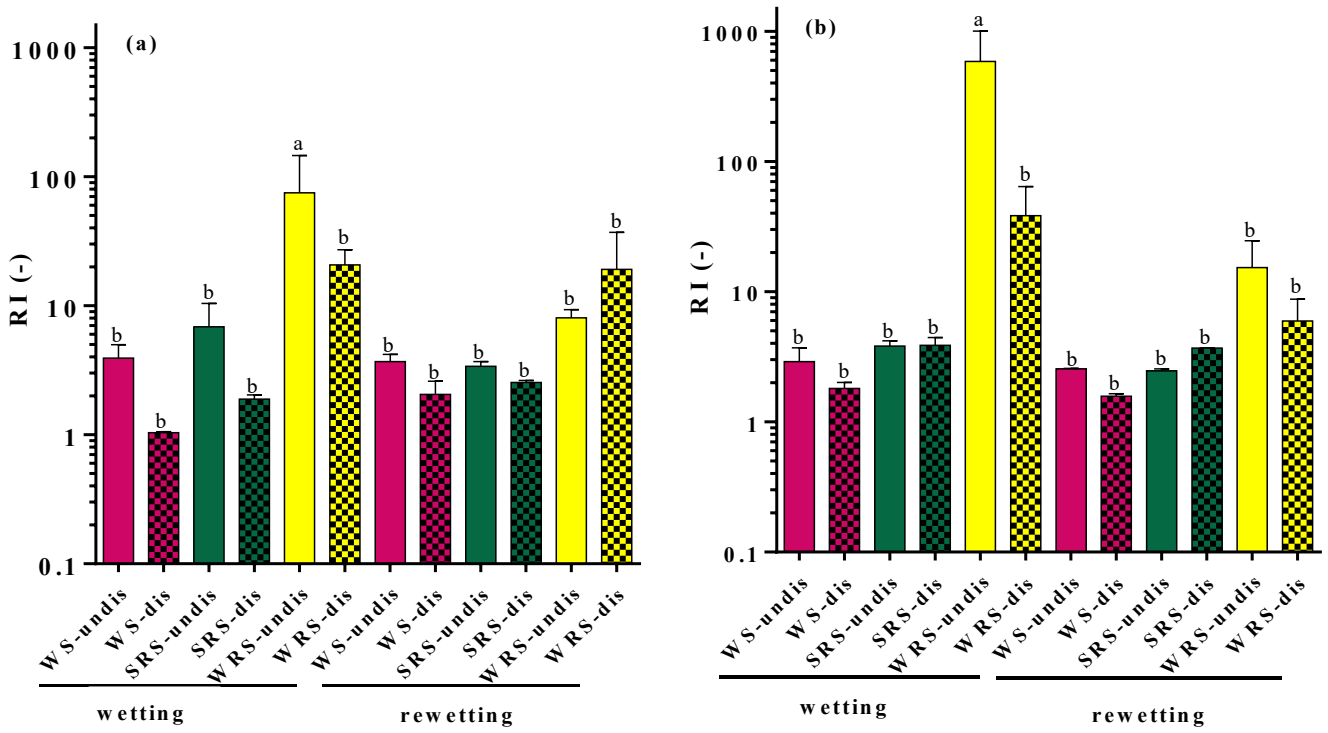

Fig. 2. Changes of Repellency index (*RI*) for the studied soils (WS: wettable soil, SRS; subcritically water-repellent soil, and WRS: water-repellent soil) treated at (a) 40 and (b) 60 °C after wetting and rewetting cycles; "dis" and "undis" are disturbed and undisturbed samples, respectively. Letters (a and b) show statistically significant differences between the variables ($p < 0.05$).

sorptivity, and time, respectively. The S can be estimated for the hydrophobic state (S_{wh}) and a nearly wettable state (S_{ww}) using the slope of "hockey-stick-like" relationship, measured at short time intervals of infiltration (Lichner et al., 2013; Sepehrnia et al., 2016). Furthermore, the conventional approach of the water repellency index by Tillman et al. (1989) (Eq.3) *RI*, was measured (Eq. 8):

$$RI = 1.95 \times S_e(-2\,\text{cm})/S_w(-2\,\text{cm}) \quad (8)$$

where S_e and S_w are the ethanol and water sorptivities, respectively. The data are illustrated in Fig. 2.

3.4. Parameters evaluated using the CTM

Several parameters including characteristic and gravity infiltration (I_{char} and I_{grav}, cm) and respective times (t_{char} and t_{grav}, cm), water and ethanol sorptivities (S_{wCTM} and S_{eCTM}, cm $h^{-0.5}$), soil-dependent shape factor for the sorptivity and gravity components (α, h^{-1}), and contribution of the gravity component to the infiltration process (ω,-) were derived from the CTM and evaluated for the soils. The results are presented in Figs. 4 and 5, and Tables 1-4.

3.5. Contact angle measurements

The sessile drop method using a CCD-equipped CA microscope (OCA 20, Data Physics, Filderstadt, Germany; Goebel et al., 2013) was applied to measure air–liquid-solid CA of the studied samples in ambient lab conditions. The measurement places one water drop (*i.e.,* 1 μl in volume) onto a dense one-grain layer fixed with a double-sided adhesive tape on a microscope slide (Bachmann et al., 2000). The CA measurements, as given as the mean of six drops, were immediately (ca. 30 mS after drop placement) performed after stabilization of the drop (initial CA, CA_i) (Bachmann et al., 2003; Goebel et al., 2013). Corresponding measurements were made for the initial CA (CA_i), wetting- and rewetting-process (CA_{we} and CA_{rewe}) which followed air-dried CA ($CA_{air\text{-}dried}$) conditions.

For the CA_{we} and CA_{rewe}, which quantify information of CA of the wetted state, a small sample was taken after each infiltration at the wetted tip area (~1 × 1 cm^2) from a depth of 0–1.5 cm (Sepehrnia et al., 2020). Samples were then shock-frozen by dipping polyethylene containers with the sample materials for 10 s in liquid nitrogen (−196 °C), followed by freeze-drying to preserve the orientation of functional groups (*i.e.,* hydrophilic and hydrophobic) of the particle interfaces during infiltration (Sepehrnia et al., 2020; Bachmann et al., 2021). The data for undisturbed and disturbed samples are given in Fig. 3.

3.6. Data analysis

The experiment was performed using a complete randomized design. The independent variables were the soils (wettable, subcritically water-repellent, and water-repellent), thermal treatments (40 °C and 60 °C), the type of samples (disturbed and undisturbed), and wetting cycle (wetting and rewetting). The dependent parameters included CA (CA_i, CA_{we}, CA_{rewe}, and $CA_{air\text{-}dried}$), *RI*, α (soil-dependent shape factor, Eq. 3), ω (the contribution of the gravity component to the infiltration process) and the WRCT including components of WRCT including the infiltration beginning time (t_b), and characteristic and gravity times (t_{char} and t_{grav}). Statistical analyses were done by two-way ANOVA (R Core Team, 2013) and the post-hoc mean comparisons were performed by the LSD test ($p < 0.05$).

4. Results

4.1. Repellency index

The average of *RI* values for the studied soils treated at 40 and 60 °C are in Fig. 2 and show the effects of soil ($p = 0.001$), sample ($p = 0.016$), temperature ($p = 0.039$) and wetting-rewetting cycle ($p = 0.008$). The minimum and maximum values of the *RI* (were measured as 1.04 (±0.017) and 586.07 (±419.8) for the disturbed wettable and

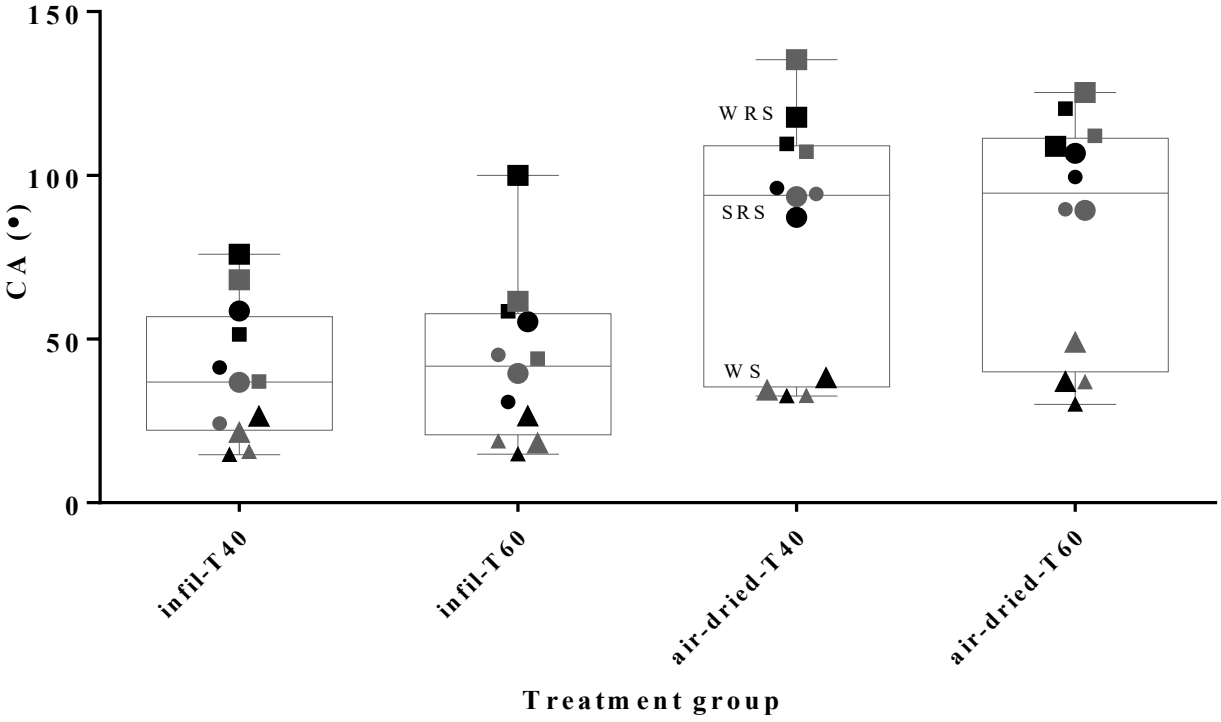

Fig. 3. Changes of contact angle (CA) for the undisturbed (*i.e.,* large symbols) and disturbed (*i.e.,* small symbols) studied soil samples (WS: wettable soil, SRS: subcritically water repellent, and WRS: water repellent soil) during infiltration (*i.e.,* infil) and the air-dried condition after infiltration (*i.e.,* air-dried) treated at 40 and 60 °C. The black and grey colors illustrate wetting and rewetting processes of infiltration, respectively.

undisturbed soils treated at 40 °C (rewetting) and 60 °C (wetting), respectively. If the wetting and rewetting processes are considered, the undisturbed samples had smaller *RI* in the rewetting process on average than the wetting counterpart. That was more notable from WS to WRS (left to right of Fig. 2). This change, however, was only observed for the WRS among the disturbed samples treated at 60 °C with no particular trend for the other samples. The other statistical interactions related to thermal treatments (*e.g.,* soil × temperature, sample × temperature, etc.) also affected *RI* values ($p < 0.05$) except for interactions between sample × temperature × wetting cycle ($p = 0.061$). If the thermal treatments are considered, the minimum *RI* values were 1.02 and 1.52 (for the WS), the medians 3.60 and 3.63 (for the SRS), and the maximum 124.86 and 883.00 (for the WRS). The *RI* values corresponded well with the general behavior reported by Weninger et al. (2019) for observations (3.53–12.40) of samples from the surface and a depth of 5 cm.

4.2. Contact angle

The CA_{we}, and $CA_{air\text{-}dried}$ ($p < 0.001$) were quite different and influenced by soil and treatment in terms of CA. The values of CA_{we} for the WS, SRS, and the WRS were 19.9° (±6.2), 41.3° (±14.1), and 62.6° (±22.8), but changed for the $CA_{air\text{-}dried}$: 36.6° (±8.8), 94.1° (±10.6), 115.5° (±22.8), respectively (Fig. 3). Interestingly, the sample mode (i.e., undisturbed vs disturbed) only affected the CA_{we} ($p < 0.001$) that was measured 52.6° (±27.90) and 35.60° (±16.04) for the undisturbed and disturbed samples, respectively, while, the values of the $CA_{air\text{-}dried}$ ($p = 0.117$) changed to 87.1° (±36.2) and 86.3° (±34.4), respectively. The thermal treatments, 40 and 60 °C, only affected the CA_{we} ($p = 0.023$), with the average of 40.1° (±21.0) and 47.7° (±26.8), while, the values for the $CA_{air\text{-}dried}$ were 83.9° (±35.9) and 89.1° (±32.6), respectively ($p = 0.90$). Furthermore, wetting and rewetting processes affected the respected CA ($p < 0.0001$), not the $CA_{air\text{-}dried}$ ($p = 0.407$), so that the values for the CA_{we} and the CA_{rewe} were 49.80° (±28) and 37.5° (±17.54), respectively. Those were 85.1° (±34.6) and 87.6° (±34.3) for the $CA_{air\text{-}dried}$ condition (Fig. 3). The changes of the CA_{we}, and $CA_{air\text{-}dried}$ values were in agreement with Bachmann et al. (2021) with regard to the SWR state of the soils.

4.3. The CTM modeling

The CTM modeling for the water and ethanol infiltration tests are in Tables 1–4. The ω values with regard to the treatments varied and were influenced by the thermal treatments ($p < 0.05$), the type of sample ($p < 0.05$), and initial soil wettability in term of CA ($p < 0.05$). The ω values smaller than 0.5 illustrate that the t_{grav} for the samples exceeded the experiment duration (Rahmati et al., 2020). For water, the mean ω values of the undisturbed and disturbed samples were 0.24 (±0.14) and 0.30 (±0.18), respectively. For ethanol, the respective values were 0.34 (±0.20), and 0.30 (±0.22). The highest ω values were obtained for the ideal case with respect to fast penetration; i.e., ethanol infiltration into the disturbed samples (Table 4). These results indicated a greater transition state for the undisturbed samples influenced by SWR as wetted by water (Tables 1 and 2) and at the same time, illustrate the physics of soil and liquid with regard to the larger ω values for the undisturbed soils wetted by ethanol (Tables 3 and 4). For water infiltration, the ω values were closer to 0.5 for the WS compared to the SRS and WRS (Tables 1 and 2) and the CTM code performance reduced as SWR appeared. The code did not run for the SRS and WRS, particularly where the extent and persistence of the samples increased (*e.g.,* undisturbed samples treated under 60 °C). To this end, we ignored persistence of the SWR as direct information for the code by omitting the time span before the beginning of the water infiltration to fit the data presented in Tables 1 and 2. Nevertheless, the time span (t_b) was valuable information indicating persistence when present (Tables 1 and 2).

The α values also showed interesting and robust information (Tables 1–4). For the undisturbed samples wetted by water (Table 1), the α values varied between 0 and 0.9 h^{-1} without having a significant difference (except for the rewetting of the WRS treated at 60 °C; −3.63 h^{-1}). In turn, larger values were found for the disturbed samples (Table 2) with a significant difference in the wetting ($p < 0.05$) if

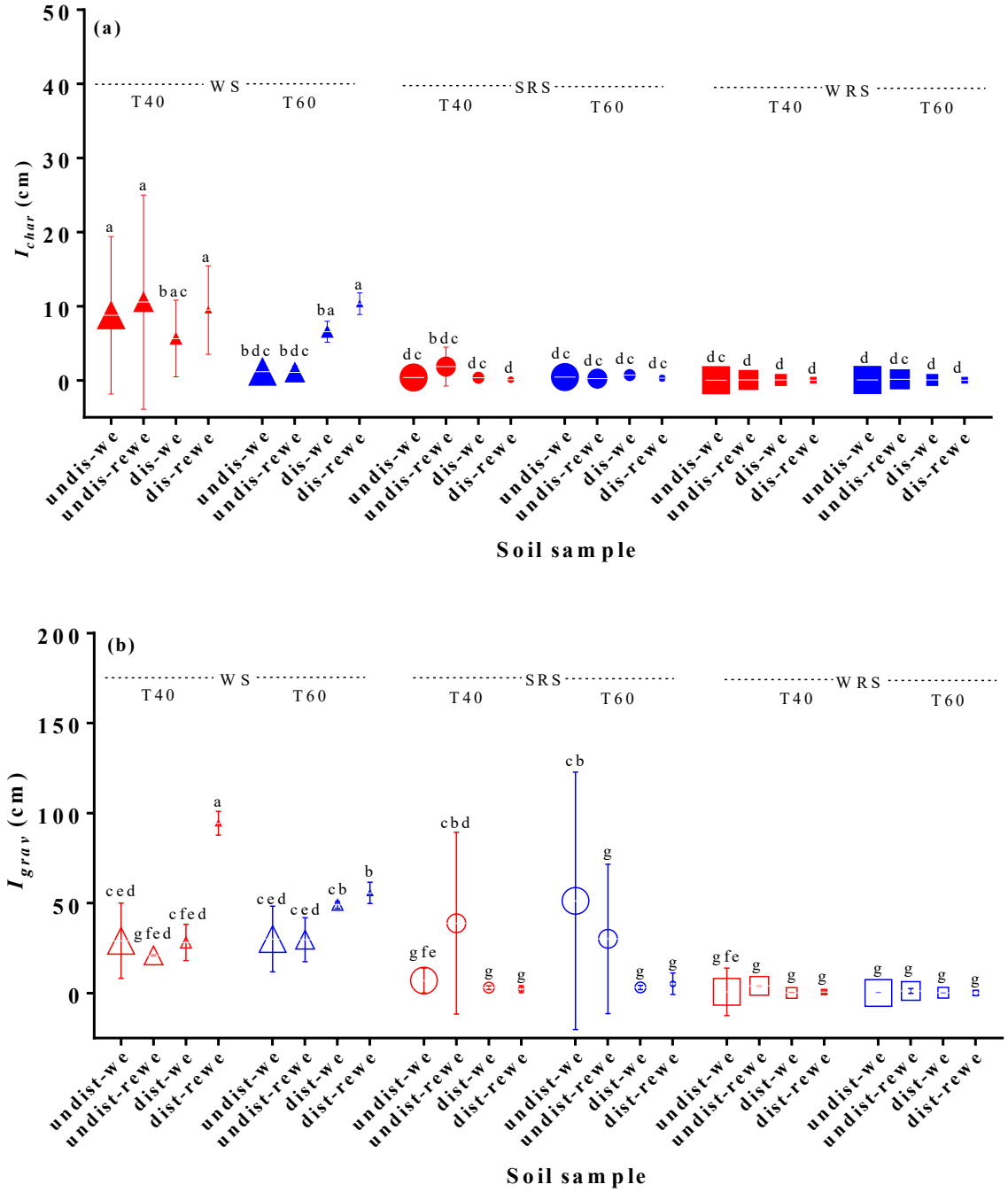

Fig. 4. Changes of characterized and gravitated infiltrations (I_{char}, I_{grav}) for water (a-b) and ethanol (c-d) modeled for the undisturbed (*i.e.,* undist) and disturbed (i.e., dist) soil samples (WS: wettable soil, SRS: subcritically water-repellent soil, and WRS: water-repellent soil) treated at 40 and 60 °C. Wetting process (we) is differentiated from the rewetting (rewe) using a larger symbol. Letters (a, b and c, etc) show statistically significant differences between the variables ($p < 0.05$).

compared with the rewetting ($p > 0.05$). On the other hand, the ω values for ethanol infiltration were 1.93–8.34 h^{-1} and 3.24–8.41 h^{-1} for the undisturbed and disturbed samples, respectively, and remained proportionally unaffected. These data (Tables 1–4) demonstrate that the α values have a high dependency on soil structure as affected by SWR (Tables 3 and 4). Rahmati et al. (2020) reported that α value is soil dependent, with smaller values for coarser textured soils. Our soils had similar texture (sandy loam, Sepehrnia et al., 2020), but surprisingly, we found that the organic matter (OM) content can also affect the α values because the data slightly showed smaller values for the high OM content soil samples (*e.g.,* SRS and WRS). Further research will reveal the effects of OM quantity and quality on α values.

4.4. Water repellency cessation time components

The time components of water and ethanol infiltration for experimental data and the results of CTM modeling are in Tables 1–4. There was no significant difference between the treatments for WS and SRS. The maximum values of the t_b were 0.48 (±0.24) and 0.237 (±0.33) h for the undisturbed and disturbed WRS, respectively, that were treated at 60 °C in the wetting process (Tables 1 and 2). Those data were also significantly different with the WS, SRS if compared with the rewetting

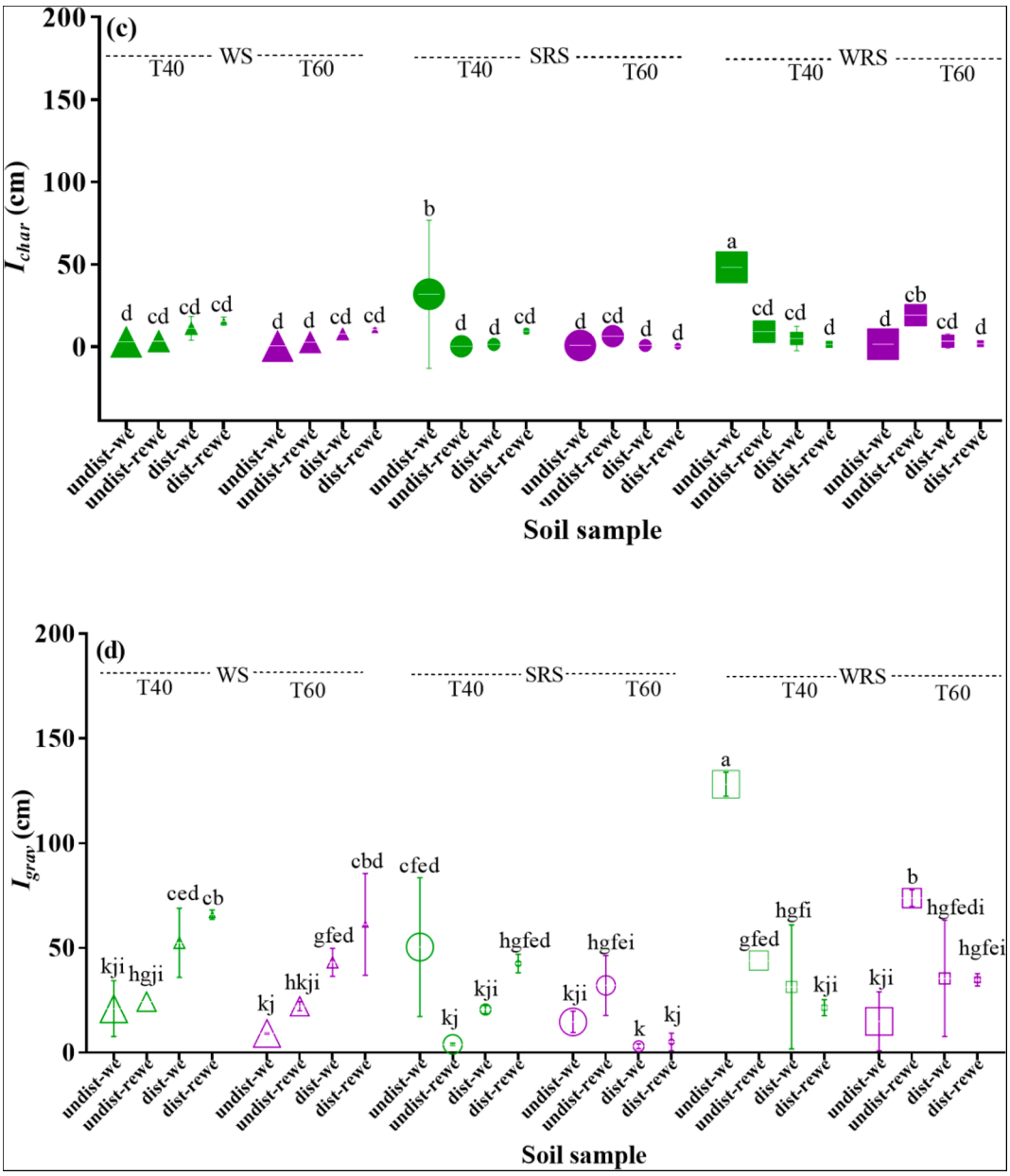

Fig. 4. (*continued*).

process ($p < 0.001$). This clearly illustrates soil structure, wetting-rewetting process, and thermal effects on the persistence of SWR. The t_b for ethanol was 0.001 h for all treatments, which was in line with liquid property and physics of soil wettability, *i.e.,* ethanol wetted the different media, regardless of the respective water wettability (Sepehrnia et al., 2020).

The t_{char} values (Tables 1–4) varied between 0 and t_{grav} as reported by Rahmati et al. (2020). For the undisturbed WS treated at 40 °C, the values of t_{char} were higher than those for 60 °C, but with regard to the standard deviation, there were no significant differences between the thermal treatments and the wetting and rewetting processes. As the SWR appeared, we still did not see a significant change for the t_{char} values of the SRS (Tables 1 and 2), but, the WRS had higher t_{char} in comparison to the WS and SRS ($p < 0.001$).

The values of t_{grav} also depended on soil and sample types, temperature, and the mode of wetting-rewetting process ($p < 0.05$). In general, the undisturbed samples had higher t_{grav} than the disturbed samples (Tables 1 and 2), the t_{grav} values were < 1 h for the latter. This clearly indicates the effect of soil structure on t_{grav}. The undisturbed WS samples reached the t_{grav} in the rewetting phase sooner than during wetting, however, the SWR, as the game changer, affected the t_{grav} values for the SRS and the WRS (Tables 1 and 2). With this, an increased trend was generally observed for the t_{grav} values of the rewetting if both undisturbed and disturbed samples are considered (Tables 1 and 2). This proportionally shows a greater dependency of the t_{grav} on soil structure affected by SWR and wetting-rewetting processes rather than the temperature. Rahamati et al. (2020) found that coarse-textured soils (*e.g.*, sandy loam; 2.60 h) have low values of t_{grav}, whereas fine textured soils have higher values of t_{grav} (*e.g.*, sandy clay; 124 h), which is in line with the physics of water infiltration into soil due to pronounced capillarity-driven flow in fine-textured soils and with our data (*i.e.,* sandy loam texture).

The WRCT data yielded from the Hockey-stick approach are also presented in Tables 1 and 2. The undisturbed WS had higher WRCT at 60 °C than at 40 °C, which corresponded with Sepehrnia et al. (2020) who found higher WRCT for higher temperature (25 and 80 °C).

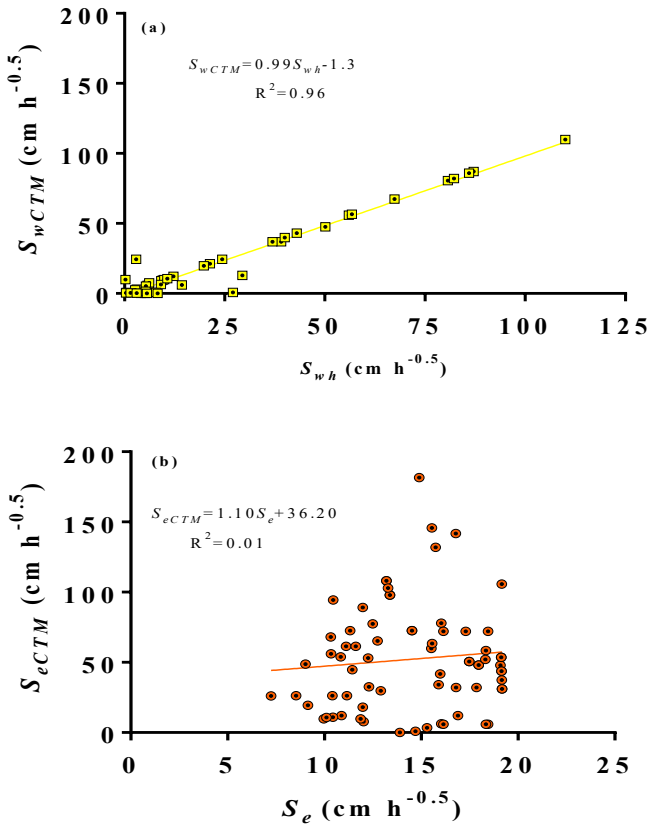

Fig. 5. Correlation between (a) water sorptivity estimated from CTM (S_{wCTM}) and Hockey-stick (S_{wh}) methods, (b) ethanol sorptivity estimated from CTM (S_{eCTM}) and the Philip's (1957) first-term equation (eq. (1)).

However, the disturbed WS treated at 40 °C with its counterpart at 60 °C had similar WRCT in the wetting and re-wetting processes. The WRCT for both the disturbed and undisturbed SRS was 0.01 h except for the rewetting at 40 °C (i.e., 0.84 h, Table 1). The WRCT for the WRS was more influenced by the mechanical pretreatments so that the undisturbed samples had higher WRCT than the disturbed ones. Further, smaller values for the WRCT were found in the rewetting compared to the wetting process. Surprisingly, with regard to the CA_i and the similar WRCT values found for the soils (Tables 1 and 2), the data prove that persistence of SWR does not necessarily depend on the CA and, most likely, depends on molecular (re)arrangement and time-dependent structure of the hydrophobic components during infiltration. Contact with water affects the quality of the organic interfaces, which are also relevant for infiltration on the macroscopic scale (Woche et al., 2017).

4.5. Characteristic and gravity infiltrations

Fig. 4 shows the I_{char} and gravity infiltration I_{grav} results of the water and ethanol tests for the soils. For water infiltration (Fig. 4a), the WS treated at 40 °C had slightly higher I_{char} compared to the 60 °C treated WS ($p < 0.05$). However, a significant difference was found between the I_{char} values of the WS, the SRS and the WRS ($p < 0.05$). For the rewetting mode, the WS showed a slight increase in I_{char}, but, not for the SRS and WRS (Fig. 4a). If the water infiltration illustrated in Fig. 4b is still considered, the latter trend was also found for the I_{grav} of the WRS and no change was observed as a consequence of the imposed treatments, indicating the dominant impacts of SWR on the physics of water movement specifically in those soils with high extent and persistence of water repellency. The differences between WS and SRS decreased for the I_{grav} (Fig. 4b). For the ethanol infiltration, however, the values of the I_{char} were mostly the same with regard to standard deviations observed for the soils. This finding is similar to I_{grav}, but, with higher variations in data for the latter (Fig. 4b), indicating that the related I_{char} is most probably affected by OM content as Sepehrnia et al. (2020) reported a higher rate of ethanol infiltration into soils with higher OM contents.

5. Discussion

5.1. The RI and CA

The soils had similar texture (*i.e.,* sandy loam) and thus as organic carbon (OC) increased from the WS (0.04 %), SRS (2.52 %) to the WRS (10.10 %) soils, these organic compounds were responsible for inducing water repellency (Sepehrnia et al., 2020). Apparently, as more mineral surfaces were coated by those compounds the greater the content of OC resulted in the greater the increase of the *RI* values (Fig. 2) (Sepehrnia et al., 2016, 2017).

Regardless of organic-mineral interactions, the *RI* variations were apparently also related to the geometry of the pore space on the flow-soil interface (Benard et al., 2018; Li et al., 2021) as higher values were found for the undisturbed samples (Fig. 2). For the rewetting process at 40 °C, if compared with the wetting counterpart, the tendency to slight increase of *RI* values for the three disturbed soils indicates wetting fronts that can meander less easily through wettable pathways between sand grains that were affected by hydrophobic materials (Bauters et al., 2000; Urbanek et al., 2015) because hydrophobic compounds are distributed more uniformly in the soil matrix. Further, at 60 °C, the unchanged *RI* values for the WS and SRS, and a considerable decrease for the WRS after rewetting, demonstrate the effect of the higher temperatures in

Table 1
Applied values of ω (the contribution of the gravity component to the infiltration process), as well as obtained characteristic (t_{char}) and gravity (t_{grav}) times, the soil-dependent shape factor of α obtained from application of characteristic time method (CTM), the infiltration beginning time (t_b), and water repellency cessation time (WRCT) over simulated water infiltration curves (tension −2 cm) for undisturbed soil samples.

Soil	process	Temperature	ω	α	t_{char}	t_{grav}	t_b	WRCT
		°C	–	h^{-1}		h		
WS	wet	40	0.49 (±0.01)	−0.32 (±0.26)	0.03 (±0.04)	1.02 (±0.81)	0.001 (0.00)	0.004 (±0.001)
WS	rewe	40	0.25 (±0.35)	−0.27 (±0.35)	0.04 (±0.06)	0.71 (±0.88)	0.001 (0.00)	0.003 (±0.002)
WS	we	60	0.29 (±0.26)	−0.82 (±0.59)	0.00 (±0.00)	2.03 (±2.47)	0.001 (0.00)	0.01 (±0.001)
WS	rewe	60	0.19 (±0.27)	−0.90 (±0.22)	0.00 (±0.00)	0.80 (±0.20)	0.001 (0.00)	0.01 (±0.001)
SRS	we	40	0.16 (±0.27)	−0.59 (±0.13)	0.003 (±0.01)	1.22 (±0.30)	0.004 (0.00)	0.01 (±0.01)
SRS	rewe	40	0.22 (±0.30)	−0.42 (±0.54)	0.000 (0.00)	9.30 (±11.90)	0.001 (0.00)	0.84 (±1.20)
SRS	we	60	0.20 (±0.28)	−0.41 (±0.54)	0.000 (0.00)	13.66 (±18.10)	0.001 (0.00)	0.01 (±0.002)
SRS	rewe	60	0.00 (±0.00)	−1.22 (±1.600)	0.000 (0.00)	4. 06 (±5.31)	0.001 (0.00)	0.01 (±0.004)
WRS	we	40	0.20 (±0.28)	−0.79 (±0.05)	0.000 (0.00)	0.88 (±0.05)	0.03 (±0.004)	2.17 (±2.48)
WRS	rewe	40	0.00 (±0.00)	−0.22 (±0.27)	0.000 (0.00)	14.68 (±18.40)	0.001 (±0.00)	0.34 (±0.01)
WRS	we	60	0.49 (±0.01)	−0.20 (±0.01)	0.53 (±0.23)	3.48 (±0.30)	0.48 (±0.24)	17.96 (±22.63)
WRS	rewe	60	0.19 (±0.26)	−3.63 (±2.54)	0.01 (±0.01)	0.26 (±0.18)	0.003 (±0.004)	0.01 (±0.002)
mean			0.22 (±0.19)	−0.82 (±0.59)	0.05 (±0.03)	4.34 (±4.90)	0.04 (±0.02)	1.80 (±2.20)

Table 2
Applied values of ω (the contribution of the gravity component to the infiltration process), as well as obtained characteristic (t_{char}) and gravity (t_{grav}) times, the soil-dependent shape factor of α obtained from application of characteristic time method (CTM), the infiltration beginning time (t_b), and water repellency cessation time (WRCT) over simulated water infiltration curves (tension − 2 cm) for disturbed soil samples.

Soil	process	Temperature	ω	α	t_{char}	t_{grav}	t_b	WRCT
		°C	–	h^{-1}			h	
WS	we	40	0.17 (±0.29)	−25.40 (±2.50)	0.000 (±0.0)	0.030 (±0.0)	0.001 (±0.0)	0.004 (±0.0)
WS	rewe	40	0.48 (±0.01)	−1.37 (±1.03)	0.005 (±0.01)	0.710 (±0.54)	0.001 (±0.0)	0.006 (±0.0)
WS	we	60	0.437 (±0.05)	−4.63 (±2.70)	0.00 (±0.0)	0.180 (±0.08)	0.001 (±0.0)	0.003 (±0.0)
WS	rewe	60	0.460 (±0.0)	−4.97 (±0.33)	0.010 (±0.0)	0.140 (±0.01)	0.001 (±0.0)	0.006 (±0.0)
SRS	we	40	0.000 (±0.0)	−27.36 (±3.10)	0.00 (±0.0)	0.027 (±0.01)	0.001 (±0.0)	0.02 (±0.004)
SRS	rewe	40	0.000 (±0.0)	−1.96 (±0.63)	0.00 (±0.0)	0.375 (±0.12)	0.001 (±0.0)	0.01 (±0.0)
SRS	we	60	0.443 (±0.06)	−7.01 (±0.67)	0.007 (±0.01)	0.097 (±0.01)	0.001 (±0.0)	0.01 (±0.004)
SRS	rewe	60	0.210 (±0.3)	−1.44 (±0.39)	0.00 (±0.0)	0.495 (±0.13)	0.001 (±0.0)	0.01 (±0.0)
WRS	we	40	0.310 (±0.27)	−12.82 (±1.70)	0.010 (±0.01)	0.053 (±0.01)	0.007 (±0.0)	0.02 (±0.01)
WRS	rewe	40	0.240 (±0.34)	−3.21 (±2.40)	0.010 (±0.01)	0.295 (±0.22)	0.006 (±0.01)	0.06 (±0.06)
WRS	we	60	0.497 (±0.01)	−0.77 (±0.60)	0.260 (±0.32)	1.82 (±2.02)	0.237 (±0.33)	1.27 (±1.01)
WRS	rewe	60	0.26 (±0.35)	−1.00 (±0.21)	0.120 (±0.06)	0.705 (±0.15)	0.120 (±0.06)	0.25 (±0.01)
mean			0.30 (±0.14)	−7.66 (±1.34)	0.035 (±0.034)	0.41 (±0.28)	0.032 (±0.034)	0.14 (±0.10)

Table 3
Applied values of ω (the contribution of the gravity component to the infiltration process), as well as obtained characteristic (t_{char}) and gravity (t_{grav}) times, the soil-dependent shape factor of α obtained from application of characteristic time method (CTM), and the infiltration beginning time (t_b), over simulated ethanol infiltration curves (tension − 2 cm) for undisturbed soil samples.

Soil	process	Temperature	ω	α	t_{char}	t_{grav}	t_b
		°C	–	h^{-1}		h	
WS	we	40	0.49 (±0.0)	−4.54 (±3.36)	0.00 (±0.0)	0.21 (±0.16)	0.001 (±0.0)
WS	rewe	40	0.50 (±0.0)	−3.24 (±0.0)	0.00 (±0.0)	0.21 (±0.0)	0.001 (±0.0)
WS	we	60	0.00 (±0.0)	−3.92 (±0.69)	0.00 (±0.0)	0.18 (±0.03)	0.001 (±0.0)
WS	rewe	60	0.43 (±0.0)	−4.00 (±1.1)	0.00 (±0.0)	0.18 (±0.04)	0.001 (±0.0)
SRS	we	40	0.33 (±0.29)	−5.32 (±6.20)	0.26 (±0.44)	0.33 (±0.37)	0.001 (±0.0)
SRS	rewe	40	0.13 (±0.23)	−6.62 (±3.22)	0.00 (±0.0)	0.13 (±0.09)	0.001 (±0.0)
SRS	we	60	0.00 (±0.0)	−4.81 (±1.89)	0.00 (±0.0)	0.16 (±0.06)	0.001 (±0.0)
SRS	rewe	60	0.49 (±0.0)	−4.39 (±1.55)	0.01 (±0.01)	0.17 (±0.06)	0.001 (±0.0)
WRS	we	40	0.49 (±0.0)	−4.41 (±0.98)	0.020 (±0.0)	0.17 (±0.04)	0.001 (±0.0)
WRS	rewe	40	0.33 (±0.28)	−8.34 (±1.52)	0.00 (±0.0)	0.10 (±0.01)	0.001 (±0.0)
WRS	we	60	0.23 (±0.33)	−3.40 (±0.10)	0.00 (±0.0)	0.21 (±0.01)	0.001 (±0.0)
WRS	rewe	60	0.49 (±0.0)	−5.40 (±0.08)	0.01 (±0.0)	0.13 (±0.0)	0.001 (±0.0)
mean			0.20 (±0.10)	−4.87 (±1.72)	0.03 (±0.04)	0.18 (±0.07)	0.001 (±0.0)

Table 4
Applied values of ω (the contribution of the gravity component to the infiltration process), as well as obtained characteristic (t_{char}) and gravity (t_{grav}) times, the soil-dependent shape factor of α obtained from application of characteristic time method (CTM), and the infiltration beginning time (t_b) over simulated ethanol infiltration curves (tension − 2 cm) for disturbed soil samples.

Soil	process	Temperature	ω	α	t_{char}	t_{grav}	t_b
		°C		h^{-1}		h	
WS	we	40	0.45 (±0.05)	−4.76 (±0.28)	0.01 (±0.01)	0.15 (±0.01)	0.001 (±0.0)
WS	rewe	40	0.49 (±0.01)	−3.44 (±0.98)	0.01 (±0.00)	0.21 (±0.06)	0.001 (±0.0)
WS	we	60	0.46 (±0.02)	−5.25 (±0.88)	0.01 (±0.01)	0.14 (±0.02)	0.001 (±0.0)
WS	rewe	60	0.49 (±0.01)	−4.24 (±0.32)	0.02 (±0.01)	0.17 (±0.01)	0.001 (±0.0)
SRS	we	40	0.00 (±0.0)	−8.41 (±1.05)	0.00 (±0.0)	0.08 (±0.02)	0.001 (±0.0)
SRS	rewe	40	0.48 (±0.01)	−7.64 (±0.02)	0.01 (±0.01)	0.09 (±0.0)	0.001 (±0.0)
SRS	we	60	0.17 (±0.03)	−7.08 (±1.30)	0.02 (±0.04)	0.10 (±0.02)	0.001 (±0.0)
SRS	rewe	60	0.49 (±0.01)	−7.15 (±0.15)	0.01 (±0.0)	0.10 (±0.0)	0.001 (±0.0)
WRS	we	40	0.17 (±0.29)	−6.43 (±1.50)	0.00 (±0.0)	0.11 (±0.03)	0.001 (±0.0)
WRS	rewe	40	0.00 (±0.0)	−8.41 (±0.25)	0.00 (±0.0)	0.08 (±0.0)	0.001 (±0.0)
WRS	we	60	0.15 (±0.25)	−5.19 (±2.62)	0.00 (±0.0)	0.16 (±0.09)	0.001 (±0.0)
WRS	rewe	60	0.00 (±0.0)	−6.27 (±1.00)	0.00 (±0.0)	0.11 (±0.01)	0.001 (±0.0)
mean			0.28 (±0.08)	−6.20 (±0.86)	0.01 (±0.01)	0.013 (±0.02)	0.001 (±0.0)

producing higher persistence of SWR (Bachmann et al., 2021, Sepehrnia et al., 2020). Sepehrnia et al. (2020) investigated changes of the *RI* for these three soils at 25 and 80 °C under different hydraulic conditions using disturbed samples and illustrated that the disturbed samples had similar *RI* values at 25 and 40 °C under the applied tension (−2 cm). However, the discrepancies in *RI* values were more pronounced between the two studies when the thermal treatments at 60 °C and 80 °C were compared with 25 °C and 40 °C for the SRS and WRS. Information on thermal efficiency to render soils hydrophobic is various and depends on the methods of measurements, the soil drying method, incubation, and temperature (Wong et al., 2020; 2021) so that complex patterns have been reported for the higher thermal efficiency (*e.g.,* Doerr et al., 2004; Bryant et al., 2005; Doerr et al., 2005; Zavala et al., 2010). Notwithstanding, Bachmann et al. (2021) reported that thermal treatment at 80 °C always rendered the soils hydrophobic.

The *RI* and CA data (CA_{we}, CA_{rewe}, and $CA_{air\text{-}dried}$) showed nonlinear

positive relationships (R^2 = 0.32–0.47) and the values of CA_{infil} (CA_{we} and CA_{rewe}) always had higher correlations (0.41–0.56*) if compared with $CA_{air\text{-}dried}$ (R^2 = 0.10–0.47). By extension, the evaluation of the sorptivity elements (S_{wh}, S_{ww}, S_w, and S_e) showed that the CA_{infil} had higher negative correlations with S_{wh} (R^2 = 0.56*) if compared with the S_{ww} (R^2 = 0.25) or S_w (R^2 = 0.41), indicating lower water sorptivity status provides the higher CA. Furthermore, the CA_{infil} had a better nonlinear positive relationship with S_e (R^2 = 0.50*) compared to $CA_{air\text{-}dried}$, illustrating that the structure of the pore system could result in higher CA values (Sepehrnia et al., 2020).

Our evaluation of SWR persistence using the CA (Fig. 3) on one hand supported the *RI* information but, on the other, revealed that the realignment of hydrophobic groups to their initial arrangement and relocation is also relevant for interpreting the measured parameters. The first evidence is that the undisturbed samples always had higher CA_{we} and CA_{rewe} than the disturbed samples for the same thermal treatments (Fig. 3), indicating the pore space geometry and SWR interactions produced a higher CA due to the inaccessibility of the hydrophobic pore portion for flowing water.

The second evidence is the very close $CA_{air\text{-}dried}$ measurements for the disturbed and undisturbed samples if any of the soils were considered. That demonstrates the realignment of the hydrophobic groups towards the initial arrangement, even after destroying the natural structure. Therefore, the results may indicate that leaching of hydrophobic coatings, and to some extent, their relocation might not be relevant under the applied tension (−2 cm).

Sepehrnia et al. (2017) observed that most leached particles from the natural colloids under saturation condition were hydrophilic. Now, given that, with repeated regular wetting cycles pathways will tend to spread gradually to extend successively to larger domains of soil until most or all of an originally water repellent region has transformed functionally to behave as wettable (Täumer et al., 2006; Wessolek et al., 2008). Therefore, the persistent hydrophobic materials/molecules might stay at surfaces and/or remain intact when separated from mineral parts during infiltration, particularly for the higher thermal treatment (60 °C). So, once the soils dried (*e.g.,* most probably to the critical water content hydrophobicity) hydrophobic functional groups are re-established at the relevant contact angle sensitive interface of a few angstroms in depth due to the re-association of polar groups to the mineral surface and non-polar tails facing outwards (Bachmann et al., 2021; Smettem et al., 2021).

Our data for the two wetting processes showed that is even possible for soils with small CA (*e.g.,* the WS, Fig. 3) and highly depended on the persistence of SWR as stressed by Bachmann et al. (2021). Bachmann et al. (2021) investigated changes of CA, in terms of the wetted-and air-dried states, through the wetting–drying cycles, as well as shock-frozen and freeze-dried treatments and confirmed a sensitive and partly reversible reorganization of the solid interfacial wetting properties that was spectroscopically related to molecular restructuring that most likely occurred due to changes in O and C content and the content of non-polar C compounds at the outermost surfaces.

5.2. The CTM code and WRCT

The CTM showed the best performance in estimating S_w for the WS, where the infiltration process showed no lag-time ($t_b < 5$ s). However, as SWR increased the code efficiency reduced because the persistence of the SWR was the main barrier to fit data with common methods. Data selection (i.e., removing the lag-time of infiltration) resulted in successful simulation runs, but still with $\omega < 0.5$ for most cases of the treatment presented in Tables 1 and 2, indicating the transition state of the infiltrated, but not fully wetted state (illustrated in Fig. 1a). Rahmati et al. (2020) reported great performance for the CTM code using a synthetic data-set and synthetic data with randomized noises. They emphasized that addition of such noise will not represent probable other important error sources such as soil layering, non-uniform infiltration, and infiltration into (dead-end) macropores. In our study, the latter was obvious in terms of SWR, which played an important role in CTM performance in terms of execution and obtaining maximum ω.

Rahmati et al. (2020) used field experimental data taken from the SWIG database (Rahmati, et al., 2018a; Rahmati, Weihermüller, and Vereecken, 2018b) to verify the feasibility of the application of the CTM to real data compared with other methods (*e.g.,* Quasi-exact implicit (QEI) formulation; Sharma et al., 1980; Haverkamp et al., 1994) and the potential impacts of experimental noise. They found that the CTM provides comparable data for S if compared with benchmark values, although, the Sharma et al. (1980) method shows slightly better robustness than CTM. In our paper, the Sharma et al. (1980) method (Eq. (7)) is termed the Hockey-stick method according to the explanation provided by Lichner et al. (2013) and Sepehrnia et al. (2016, 2017) to estimate S_{wh}. Our data revealed that the S_w from the CTM had an excellent agreement with S_{wh} (R^2 = 0.96) (Fig. 5a) following, the t_{char} and t_b (R^2 = 0.99) (Tables 1 and 2). This demonstrates that for the soils with less extent and persistence of SWR (i.e., most probably having ω = 0.5), the predicted S_w by CTM can be used to estimate RI_m (Sepehrnia et al., 2017). However, we could not find a correlation between Se and S_{eCTM}. This may limit the CTM for ethanol infiltration data and estimation of *RI* (Fig. 5b). Furthermore, simulation of water infiltration proved that the I_{char} values (Fig. 4a) and the I_{grav} for the high persistence cases (WRS, Fig. 4b) were considerably reduced, whereas those values were only influenced by soil type and OM content for the ethanol data (Fig. 4c and 4d). Keep in mind that the use of CTM omits the necessity of arbitrariness in limits of time selection for the S_w and S_e estimation as stressed by Rahmati et al. (2020).

Modeling water flow characteristics through studied soils using HYDRUS 2D/3D with regard to the boundary conditions of the experiments provided the applicability of the CTM to modelled 3D infiltration characteristics (see supplementary data). By extension, the data illustrated that water flow (i.e., pressure head and water content changes) was successfully modeled for the slight to moderate persistence of water repellency states (t_b: 0.001 h for the WS and 0.004 h for the SRS soils treated at 40 °C, respectively) while HYDRUS 1D failed to simulate severe water repellency (i.e., long time-lag for water infiltration; t_b: 0.48 h for the WRS treated at 60 °C). Therefore, the future challenge is to implement the persistence of SWR into the HYDRUS 1D interface and the CTM code and to prove how well the above extension works for different soils.

6. Conclusions

For the first time the applicability of the characteristic time method (CTM) to estimate sorptivity (S) of water-repellent soils that exhibit the typical characteristics of the water repellency cessation time (WRCT) was evaluated. The CTM provided valid predictions of S_w and S_e for the soils. The predicted S_w were highly correlated with S_{wh}. However, the code did not execute for the SRS and WRS with high persistence of water repellency. We believe that modality of the data were influenced by the specific nature of SWR even when analyzing almost noise-free experimental data evaluated with high precision. It could fit infiltration data with slight to moderate persistence of water repellency states. Transformation of the time axis according to persistence of SWR resulted in having an accurate estimation of S_w that was highly correlated with S_{wh} measured from the Hockey-stick method.

We showed that the persistence of SWR played a key role in the success of the CTM code execution. The key points of our findings with regard to the treatments can be summarized as follows.

- Thermal treatments, wetting, rewetting, and air-drying processes affected the extent (*i.e., RI*) and persistence of SWR (*i.e.,* CA).
- Soil structure coupled with SWR produced higher CA (CA_i, CA_{we}, and CA_{rewe}).

- The extent and persistence of SWR control the characteristic and gravity infiltration part (I_{char} and I_{grav}) so that the studied SRS and WRS remained at the transition state during infiltration (i.e., the ω values<0.5).
- The time components (WRCT, t_b, t_{char}, and t_{grav}) showed the effects of extent and persistence of SWR even for those with small CA.

Further research to update the executive code will warranty the CTM application in the water repellent-affected soils with high persistence of water repellency We suggest updating the CTM code to obtain a protocol for the mathematical prediction of the WRCT and to minimize arbitrariness in selection of S_{wh} and S_{ww}. Corresponding parameters are needed to simulate water infiltration into water-repellent soil with respect to initial water repellency level and persistence.

Declaration of Competing Interest

The authors declare that they have no known competing financial interests or personal relationships that could have appeared to influence the work reported in this paper.

Data availability

Data will be made available on request.

Acknowledgments

We thank the Alexander von Humboldt Foundation for financial support of this project and donating post-doctoral fellowship to the first author. We thank Susanne K. Woche, Hanna Böhme, and Martin Volkmann for their assistance with soil sampling, sample preparation, and laboratory analysis. The authors greatly appreciate Prof. Mark Coyne, University of Kentucky, USA for proofreading the draft of the article.

Appendix A. Supplementary data

Supplementary data to this article can be found online at https://doi.org/10.1016/j.geoderma.2022.116126.

References

Alagna, V., Iovino, M., Bagarello, V., Mataix-Solera, J., Lichner, L., 2019. Alternative analysis of transient infiltration experiment to estimate soil water repellency. Hydrol. Process 33 (4), 661–674.
Arye, G., Nadav, I., Chen, Y., 2007. Short-term reestablishment of soil water repellency after wetting: Effect on capillary pressure–saturation relationship. Soil Sci. Soc. Am. J. 71 (3), 692–702.
Bachmann, J., Woche, S.K., Goebel, M.-O., Kirkham, M.B., Horton, R., 2003. Extended methodology for determining wetting properties of porous media. Water Resour. Res. 39, 1353.
Bachmann, J., Deurer, M., Arye, G., 2007. Water-repellent soil: Development of a contact angle–dependent water-retention model. Vadose Zone J. 6, 436–445.
Bachmann, J., Krueger, J., Goebel, M.O., Heinze, S., 2016. Occurrence and spatial pattern of water repellency in a beech forest subsoil. J. Hydrol. Hydromech. 64, 100–110.
Bachmann, J., Söffker, S., Sepehrnia, N., Goebel, M.-O., Woche, S.K., 2021. The effect of temperature and wetting–drying cycles on soil wettability: Dynamic molecular restructuring processes at the solid–water–air interface. Eur. J. Soil Sci. 72 (5), 2180–2198.
Bauters, T.W.J., Steenhuis, T.S., DiCarlo, D.A., Nieber, J.L., Dekker, L.W., Ritsema, C.J., Parlange, J.-Y., Haverkamp, R., 2000. Physics of water repellent soils. J. Hydrol. 231-232, 233–243.
Beatty, S.M., Smith, J.E., 2013. Dynamics of soil water repellency and infiltration in post-wildfire soils. Geoderma 192, 160–172.
Beatty, S.M., Smith, J.E., 2014. Infiltration of water and ethanol solutions in water repellent post wildfire soils. J. Hydrol. 514, 233–248.
Benard, P., Zarebanadkouki, M., Hedwig, C., Holz, M., Ahmed, M.A., Carminati, A., 2018. Pore-scale distribution of mucilage affecting water repellency in the rhizosphere. Vadose Zone J. 17 (1), 170013.
Bryant, R., Doerr, S.H., Helbig, M., 2005. The effect of oxygen deprivation on soil hydrophobicity during heating. Int. J. Wildland Fire 14, 449–455.
Daniel, N.R.R., Uddin, S.M.M., Harper, R.J., Henry, D.J., 2019. Soil water repellency: A molecular-level perspective of a global environmental phenomenon. Geoderma 338, 56–66.
de Jonge, L.W., Moldrup, P., Jacobsen, O.H., 2007. Soil-water content dependency of water repellency in soils: Effect of crop type, soil management, and physical-chemical parameters. Soil Sci. 172, 577–588.
Dekker, L.W., Ritsema, C.J., 1994. How water moves in a water repellent sandy soil. I. Potential and actual water repellency. Water Resour. Res. 30, 2507–2517.
Dekker, L.W., Ritsema, C.J., Oostindie, K., Moore, D., Wesseling, J.G., 2009. Methods for determining soil water repellency on field-moist samples. Water Resour. Res. 45, W00D33. https://doi.org/10.1029/2008WR007070.
Doerr, S.H., 1998. On standardizing the "water drop penetration time" and the "molarity of ethanol droplet" techniques to classify soil hydrophobicity: A case study using medium textured soils. Earth Surf. Processes Landforms 23, 663–668.
Doerr, S.H., Thomas, A.D., 2000. The role of soil moisture in controlling water repellency: new evidence from forest soils in Portugal. J. Hydrol. 231, 134–147.
Doerr, S.H., Blake, W.H., Shakesby, R.A., Stagnitti, F., Vuurens, S.H., Humphreys, G.S., Wallbrink, P., 2004. Heating effects on water repellency in Australian eucalypt forest soils and their value in estimating wildfire soil temperatures. Int. J. Wildland Fire 13 (2), 157.
Doerr, S.H., Llewellyn, C.T., Douglas, P., Morley, C.P., Mainwaring, K.A., Haskins, C., Johnsey, L., Ritsema, C.J., Stagnitti, F., Allinson, G., Ferreira, D., Keizer, J.J., Ziogas, A.K., Diamantis, J., 2005. Extraction of compounds associated with water repellency in sandy soils of different origin. Soil Res. 43 (3), 225.
Flores-Mangual, M.L., Lowery, B., Bockheim, J.G., Pagliari, P.H., 2011. A revised water drop method for assessing soil water repellency. Soil Sci. 176, 124–128.
Goebel, M.-O., Bachmann, J., Reichstein, M., Janssens, I.A., Guggenberger, G., 2011. Soil water repellency and its implications for organic matter decomposition – Is there a link to extreme climatic events? Glob. Change Biol. 17, 2640–2656.
Goebel, M.O., Woche, S.K., Abraham, P.M., Schaumann, G.E., Bachmann, J., 2013. Water repellency enhances the deposition of negatively charged hydrophilic colloids in a water saturated sand matrix. Colloids Surf. A 431, 150–160.
Hallett, P.D., Baumgartl, T., Young, I.M., 2001. Subcritical water repellency of aggregates from a range of soil management practices. Soil Sci. Soc. Am. J. 65 (1), 184–190.
Hallett, P.D., Young, I.M., 1999. Changes to water repellence of soil aggregates caused by substrate-induced microbial activity. Eur. J. Soil Sci. 50 (3), 35–40.
Hardie, M.A., Cotching, W.E., Doyle, R.B., Lisson, S., 2012. Influence of climate, water content and leaching on seasonal variations in potential water repellence. Hydrol. Process 26 (13), 2041–2048.
Haverkamp, R., Ross, P.J., Smettem, K.R.J., Parlange, J.Y., 1994. Three-dimensional analysis of infiltration from the disc infiltrometer: 2. Physically based infiltration equation. Water Resour. Res. 30 (11), 2931–2935.
Hermansen, C., Moldrup, P., Müller, K., Jensen, P.W., van den Dijssel, C., Jeyakumar, P., de Jonge, L.W., 2019. Organic carbon content controls the severity of water repellency and the critical moisture level across New Zealand pasture soils. Geoderma 338, 281–290.
Iovino, M., Pekárová, P., Hallett, P.D., Pekár, J., Lichner, Ľ., Mataix-Solera, J., Alagna, V., Walsh, R., Raffan, A., Schacht, K., Rodný, M., 2018. Extent and persistence of soil water repellency induced by pines in different geographic regions. J. Hydrol. Hydromech. 66, 360–368.
Lassabatère, L., Angulo-Jaramillo, R., Soria Ugalde, J.M., Cuenca, R., Braud, I., Haverkamp, R., 2006. Beerkan estimation of soil transfer parameters through infiltration experiments: BEST. Soil Sci. Soc. Am. J. 70 (2), 521–532.
Lesk, C., Rowhani, P., Ramankutty, N., 2016. Influence of extreme weather disasters on global crop production. Nature 529 (7584), 84–87.
Li, S., Lu, J., Liang, G., Wu, X., Zhang, M., Plougonven, E., Wang, Y., Gao, L., Abdelrhman, A.A., Song, X., Liu, X., Degré, A., 2021. Factors governing soil water repellency under tillage management: the role of pore structure and hydrophobic substances. Land Degrad. Dev. 32 (2), 1046–1059.
Lichner, L., Hallett, P.D., Drongova, Z., Czachor, H., Kovacik, L., Mataix-Solera, J., Homolak, M., 2013. Algae influence the hydrophysical parameters of a sandy soil. Catena 108, 58–68.
Liebmann, P., Mikutta, R., Kalbitz, K., Wordell-Dietrich, P., Leinemann, T., Preusser, S., Mewes, O., Perrin, E., Bachmann, J., Don, A., Kandeler, E., Marschner, B., Schaarschmidt, F., Guggenberger, G., 2022. Biogeochemical limitations of carbon stabilization in forest subsoils. J. Plant Nutr. Soil Sci. 185 (1), 35–43.
Mao, J., Nierop, K.G.J., Dekker, S.C., Dekker, L.W., Chen, B., 2019. Understanding the mechanisms of soil water repellency from nanoscale to ecosystem scale: a review. J. Soils Sediments 19 (1), 171–185.
Philip, J.R., 1957. The theory of infiltration: 1. The infiltration equation and its solution. Soil Sci. 83 (5), 345–358.
Philip, J.R., 1969. Theory of infiltration. Adv. Hydrosci. 5, 215–296.
Rahmati, M., Weihermüller, L., Vereecken, H., 2018b. Soil Water Infiltration Global (SWIG) database. PANGAEA. doi:10.1594/PANGAEA.885492.
Rahmati, M., Weihermüller, L., Vanderborght, J., Pachepsky, Y.A., Mao, L., Sadeghi, S. H., Vereecken, H., 2018a. Development and analysis of the Soil Water Infiltration Global database. Earth Syst. Sci. Data 10, 1237–1263.
Rahmati, M., Vanderborght, J., Šimunek, J., Vrugt, J.A., Moret-Fernández, D., Latorre, B., Lassabatere, L., Vereecken, H., 2020. Soil hydraulic properties estimation from one-dimensional infiltration experiments using characteristic time concept. Vadose Zone J. 19, e20068.
Ritsema, C.J., Nieber, J.L., Dekker, L.W., Steenhuis, T.S., 1998. Stable or unstable wetting fronts in water repellent soils — effect of antecedent soil moisture content. Soil Tillage Res. 47 (1-2), 111–123.

Sepehrnia, N., Hajabbasi, M.A., Afyuni, M., Lichner, Ľ., 2016. Extent and persistence of water repellency in two Iranian soils. Biologia 71 (10), 1137–1143.
Sepehrnia, N., Hajabbasi, M.A., Afyuni, M., Lichner, L., 2017. Soil water repellency changes with depth and relationship to physical properties within wettable and repellent soil profiles. J. Hydrol. Hydromech. 65, 99–104.
Sepehrnia, N., Woche, S.K., Goebel, M.-O., Bachmann, J., 2020. Development of a universal microinfiltrometer to estimate extent and persistence of soil water repellency as a function of capillary pressure and interface chemical composition. J. Hydrol. Hydromech. 68 (4), 392–403.
Sharma, M.L., Gander, G.A., Hunt, C.G., 1980. Spatial variability of infiltration in a watershed. J. Hydrol. 45 (1-2), 101–122.
Smettem, K.R.J., Rye, C., Henry, D.J., Sochacki, S.J., Harper, R.J., 2021. Soil water repellency and the five spheres of influence: A review of mechanisms, measurement and ecological implications. Sci. Total Environ. 787, 147429.
Täumer, K., Stoffregen, H., Wessolek, G., 2006. Seasonal dynamics of preferential flow in a water repellent soil. Vadose Zone J. 5, 405–411.
Tillman, R.W., Scotter, D.R., Wallis, M.G., Clothier, B.E., 1989. Water-repellency and its measurement by using intrinsic sorptivity. Aust. J. Soil Res. 27, 637–644.
Urbanek, E., Walsh, R.P.D., Shakesby, R.A., 2015. Patterns of soil water repellency change with wetting and drying: the influence of cracks, roots and drainage conditions. Hydrol. Process 29, 2799–2813.
Van Rossum, G., Drake, F.L., 2009. Python 3 Reference Manual. CreateSpace, Scotts Valley, CA.
Wessolek, G., Schwärzel, K., Greiffenhagen, A., Stoffregen, H., 2008. Percolation characteristics of a water-repellent sandy forest soil. Eur. J. Soil Sci. 59, 14–23.
Woche, S.K., Goebel, M.-O., Mikutta, R., Schurig, C., Kaestner, M., Guggenberger, G., Bachmann, J., 2017. Soil wettability can be explained by the chemical composition of particle interfaces - An XPS study. Sci. Rep. 7, 42877.
Wong, E.V.S., Ward, P.R., Murphy, D.V., Leopold, M., Barton, L., 2020. Vacuum drying water-repellent sandy soil: Anoxic conditions retain original soil water repellency under variable soil drying temperature and air pressure. Geoderma 372, 114385.
Wong, E.V.S., Ward, P.R., Murphy, D.V., Leopold, M., Barton, L., 2021. Soil water repellency in sandy soil depends on the soil drying method, incubation temperature and specific surface area. Geoderma 402, 115264.
Zavala, L.M., Granged, A.J.P., Jordán, A., Bárcenas-Moreno, G., 2010. Effect of burning temperature on water repellency and aggregate stability in forest soils under laboratory conditions. Geoderma 15, 366–374.